
Differentiable Simulations for Enhanced Sampling of Rare Events

Martin Šípka^{1,2} Johannes C. B. Dietschreit¹ Rafael Gómez-Bombarelli¹

Abstract

We develop a novel approach to enhanced sampling of chemically reactive events using differentiable simulations. We merge the reaction path discovery and biasing potential computation into one end-to-end problem and solve it by path-integral optimization. The techniques developed contribute directly to the understanding and usability of differentiable simulations as we introduce new approaches and prove the stability properties of our method.

1. Introduction

The idea to differentiate through simulations comes naturally from the optimization of path-dependent quantities. If the minimization of a loss function cannot be formulated separately for every frame in a trajectory, but only for the entire path, then optimization has to include the whole path leading up to each frame. For gradient descent, we must obtain the gradient of the loss with respect to the controllable parameters along the entire path. Simulations that are fully differentiable have been developed for optimization, control, and learning of motion (Degraeve et al., 2016; de Avila Belbute-Peres et al., 2018; Hu et al., 2019; 2020) but also for the learning and optimization of quantities of interest in molecular dynamics (Wang et al., 2020; Ingraham et al., 2019; Greener & Jones, 2021). While the results are often promising, it is well known and summarized in (Metz et al., 2021) that naïvely backpropagated gradients may not lead to a useful parameter update. Gradient vanishing, or on the other hand, explosions, do not allow their efficient use and are an open challenge. The problem is well-known to be associated with the spectrum of the system’s Jacobian (Metz et al., 2021; Galimberti et al., 2021) and closely connected to the chaotic nature of the simulated equations. Therefore, in order to employ path differentiation, we need to find solutions to these limitations.

In this paper, we modify the framework of differentiable simulations for the investigation of reactive chemical events. A chemical reaction can be viewed as a transition from one depression (reactant) on the potential energy surface (PES) to another (product). The two energy wells are separated by a potential energy barrier that the system has to surmount. It is only possible to estimate said reaction barrier, and therefore the likelihood of the reaction, once the transition mechanism has been unveiled. The major obstacle in determining the mechanism, i.e., the most likely path connecting reactant and product, lays in its high dimensional nature. Typical reactive systems under study might have degrees of freedom on the orders of hundreds, thousands, or even hundreds of thousands in the case of large solvated systems. On high dimensional PESs, it is impossible to explore paths blindly, and it is necessary to introduce some form of intuition. Extensive sampling of regions with high free energies (Chipot & Pohorille, 2007; Chipot, 2014) is needed and simple sampling algorithms such as e.g., Molecular dynamics (MD) or Monte-Carlo (MC) often remain trapped in (meta)stable regions, leading to a non-ergodic sampling of configuration space.

The problem has been commonly addressed by splitting it into two seemingly easier sub-tasks. First, the so-called collective variables (CVs) are identified, which act as a dimensionality reduction technique. Due to the exponential growth of computational cost, known as the curse of dimensionality, (Bellman, 1967; Köppen, 2000) one picks one to three degrees of freedom (DoF) that represent the reaction, while all others are expected to be noise. In other words, the CVs should be selected as those DoF, which are much slower than all others and which fully describe the rare transition event. Once equipped with a low dimensional map, we study the event by means of enhanced sampling (Torrie et al., 1977; Darve & Pohorille, 2001; Laio & Parrinello, 2002; Abrams & Bussi, 2013; Spiwok et al., 2015; Valsson et al., 2016) usually by introducing a biasing potential. This biasing potential is a function of the identified CVs and modifies the original Hamiltonian by lowering the reaction barrier and enhancing exploration along the chosen degrees of freedom. If CVs and enhanced sampling are chosen well, the biased dynamics will show reactive events, and subsequent analysis of the biasing potential will unravel the properties of the reactive dynamics.

¹Massachusetts Institute of Technology, 77 Massachusetts Ave, Cambridge, MA 02139 ²Mathematical Institute, Faculty of Mathematics and Physics, Charles University, Sokolovská 83, 186 75 Prague. Correspondence to: Rafael Gómez-Bombarelli <rafagb@mit.edu>.

While there are standard packages and general, widely used methods helping us to solve the second problem, the first part - collective variables identification is still largely a manual task with automatic tools just emerging. (Sultan & Pande, 2018; Mendels et al., 2018; Wehmeyer & Noé, 2018; Wang et al., 2019; Bonati et al., 2020; Wang & Tiwary, 2021; Sun et al., 2022; Šípka et al., 2022) The use of machine learning for the automatic identification of important degrees of freedom in complicated and unstructured systems seems like a natural choice, yet it comes with many pitfalls and sharp edges. The main problem of the method is referred to as a chicken-and-egg situation. To properly learn the correct CVs for the reaction mechanism, training data close to the transition state is needed. However, it is difficult to obtain such data when the transition itself is what one is trying to discover in the first place. To solve this problem, iterative improvements of the CVs were introduced. (Chen et al., 2018b) Another potential issue of the CVs identification *a priori* is the inability to correct the collective variables on the fly. This means that once we have identified some CVs, we must be certain that the CV function is properly defined and well behaved in all regions. This places a significant burden on the CV identification method as it needs to be constructed in a way that any point from the transition path does not result in unexpected CV values and stays well within the desired range. A hard task, for example, for a neural network.

Employing differentiable simulations, we aim to create a method merging two steps of reaction barrier exploration. We define a differentiable loss function that, when minimized, results in a biasing potential promoting desired reactive events. The loss gradient behaviour is thoroughly investigated, and a mechanism to control its fluctuations and magnitude is proposed. The manuscript is structured as follows. In Section 2 we define molecular dynamics simulations biased with a learnable potential, introduce a formalism to describe chemical reactions using path integrals, and outline the concept of differentiable simulations. We discuss the challenges and limitations of using differentiable simulations in their current state in Section 3. In the same section we propose two novel techniques to resolve the outlined limitations. Firstly, partially detaching the state variable from the computational graph and thereby pruning the computational graph, which enables the linearization of the equations, making it possible to keep the arising gradients provably finite. Secondly, graph mini-batching further stabilizes the training and allows working with lower learning rates and a higher number of small updates. Finally, we demonstrate the usefulness of differentiable simulations in the context of chemical reactions by training the bias function promoting barrier crossing for low dimensional numerical examples as well as the prototypical alanine-dipeptide molecule.

2. Problem Definition

Molecular dynamics is commonly used to explore reaction processes on a detailed level of individual atoms. Let the column vector $\mathbf{x} \in \mathbb{R}^N$ denote the mass-weighted coordinates of the system and \mathbf{p} the conjugated momenta. The particle motion is simulated using Hamiltonian equations with potential energy function $U_0(\mathbf{x})$.

$$\begin{aligned}\dot{\mathbf{x}}(t) &= \mathbf{p}(t) \\ \dot{\mathbf{p}}(t) &= -\frac{\partial U_0(\mathbf{x}(t))}{\partial \mathbf{x}}\end{aligned}\quad (1)$$

These equations conserve energy and are purely reversible with respect to time. However, it is common in molecular modeling not to work with the micro-canonical ensemble but rather with the canonical ensemble that conserves temperature (Callen & Scott, 1998). To do so, a thermostat is coupled to the system, keeping it close to a preset temperature. In this work, we choose the Langevin thermostat because of its implementational simplicity and its favorable properties with respect to differentiating along the computational graph, as will be shown later. In Langevin dynamics, the thermostat is coupled to the system through the friction constant γ .

The presence of a thermostat alone, however, does not guarantee that reaction events can be observed on typical simulation scales, as transitions are extremely rare. Therefore, to enable barrier crossing we modify the PES with a learnable bias term $B(\mathbf{x}, \theta)$

$$U(\mathbf{x}, \theta) = U_0(\mathbf{x}) + B(\mathbf{x}, \theta), \quad (2)$$

where the biasing function is parameterized by θ , which we aim to train to increase the frequency of reaction events. The biased dynamics evolve according to

$$\begin{aligned}\dot{\mathbf{x}}(t) &= \mathbf{p}(t) \\ \dot{\mathbf{p}}(t) &= -\frac{\partial U(\mathbf{x}(t))}{\partial \mathbf{x}} - \gamma \mathbf{p}(t) + \sqrt{2\gamma k_B T} \mathbf{R}(t),\end{aligned}\quad (3)$$

where k_b is the Boltzmann constant, T the absolute temperature of the bath, and $\mathbf{R}(t)$ a Gaussian process.

2.1. Process of chemical reactions

It is often suitable to use general curvilinear coordinates and not simply Cartesian or mass-weighted coordinates to describe reactions. Common are internal coordinates such as interatomic distances, angles, or dihedrals, as they are invariant with respect to system rotation and translation. These special coordinates are denoted with $\boldsymbol{\xi}(\mathbf{x}) \in \mathbb{R}^M$ and $M \leq N$.

The wells W of reactant (-1) and product (1), divided by a reaction barrier, are characterized by the set of points Γ_α

($\alpha = -1, 1$), which correspond to the equilibrium configurations in reactants and products, i.e., we expect an unbiased simulation on the PES $U_0(\mathbf{x})$, to stay in these basins with a very high probability. To model which points belong to the basin, we approximate the wells with a multivariate normal distribution. From short, unbiased simulations, we estimate mean $\boldsymbol{\mu}_\alpha$ and covariance matrix $\boldsymbol{\Sigma}_\alpha$. We consider a point to be part of a well if the probability of the point belonging to the distribution is above some chosen probability threshold.

$$W_\alpha = \{ \mathbf{x} \mid (\boldsymbol{\xi}(\mathbf{x}) - \boldsymbol{\mu}_\alpha)^T \boldsymbol{\Sigma}_\alpha^{-1} (\boldsymbol{\xi}(\mathbf{x}) - \boldsymbol{\mu}_\alpha) < \epsilon \}, \quad (4)$$

where epsilon can be obtained from χ^2 distribution. The indicator function for a well is

$$\mathbb{1}_\alpha(\mathbf{x}) = \begin{cases} 1 & \text{for } \mathbf{x} \in W_\alpha \\ 0 & \text{for } \mathbf{x} \notin W_\alpha. \end{cases} \quad (5)$$

In this manuscript, we only consider transitions between two wells, W_{-1} and W_1 . Additional basins would be handled analogously. The (escape) probability p_α , within a specified time interval (t_0, t_e) of a transition $W_{-\alpha} \rightarrow W_\alpha$ is defined as

$$p_\alpha = P \left(\int_{t_0}^{t_e} \mathbb{1}_\alpha(\mathbf{x}(t)) dt > 0 \mid \mathbf{x}(t_0) \in W_{-\alpha} \right), \quad (6)$$

where t_0 is the start and t_e the end time of the trajectory \mathbf{X} . This can be understood as the probability of finding at least one point in W_α of a trajectory that has started in $W_{-\alpha}$. Our objective is to increase both p_1 and p_{-1} simultaneously to a level where both events can be observed frequently on a typical simulation time scale.

2.2. Optimizing the probability

The form of the probability in (6) is not usable for differentiable optimization and needs to be recast to a differentiable, continuous form. Under suitable regularity conditions, we can replace the expression of (6) with

$$p_\alpha = P \left(\sup_{t < t_e} \mathbb{1}_\alpha(\mathbf{x}(t)) > 0 \mid \mathbf{x}(t_0) \in W_{-\alpha} \right). \quad (7)$$

We can then define a soft loss function that is continuous everywhere and differentiable for any trajectory \mathbf{X} with $\mathbf{x}(t_0) \in W_{-\alpha}$ as

$$L = L_{\xi_\alpha} = \begin{cases} 0 & \text{if } \exists \mathbf{x}(t) \in W_\alpha \\ \min_{t_0 < t < t_e} (\boldsymbol{\xi}(\mathbf{x}(t)) - \boldsymbol{\xi}_\alpha)^2 & \text{otherwise} \end{cases}, \quad (8)$$

where for each trajectory a random single $\boldsymbol{\xi}_\alpha \in \Gamma_\alpha$ is selected for the loss function by running a short, unbiased simulation. Minimizing this loss function is equivalent to maximizing the probability (6). In the following Section,

we will define a method that can be employed to minimize (8). Note that the loss function is defined only for one point of the trajectory and is influenced by the dynamics of every point that proceeds it.

2.3. Differentiable simulations

For the problem at hand, the parameters θ of the bias potential (2) have to be optimized such that the loss (8) is minimal. For a differentiable simulation, the information that we gain by differentiating the loss function at the point where it is defined can be used for optimization along the whole trajectory. While we could proceed by considering the simulation as a forward method, saving the computational graph for the entire path, it would be extremely memory-demanding. Instead, the optimization process can be conveniently reformulated using the adjoint equation and resulting adjoint vectors. We employ the framework and notation adapted recently for neural networks (Chen et al., 2018a) from the original work by Lev et al. (Lev Semenovich Pontryagin et al., 1962)

We propagate the state $\mathbf{z}(t) = (\mathbf{x}(t), \mathbf{p}(t))$ using the biased Langevin dynamics where the right side of (3) shall be denoted as $f(\mathbf{z}(t), \theta) = \dot{\mathbf{z}}(t)$. Propagating $\mathbf{z}(t)$ using $f(\mathbf{z}(t))$ is called the *forward process*. Notice that $f(\mathbf{z}(t))$ has no explicit time dependence (only through $\mathbf{z}(t)$). We define the adjoint vectors for this equations as

$$\mathbf{a}(t) = \frac{\partial L}{\partial \mathbf{z}(t)}, \quad (9)$$

To solve (9) we introduce the new time $\tau \in (0, \tau_e)$ such that $\mathbf{z}(\tau = 0) = \mathbf{z}(t = t_e)$ and $\mathbf{z}(\tau = \tau_e) = \mathbf{z}(t = 0)$. This backward flowing time reflects that the loss is not influenced by any points further in forward time.

In forward moving time t , the adjoint vectors obey the equations

$$\begin{aligned} \mathbf{a}(t_e) &= \frac{\partial L}{\partial \mathbf{z}(t_e)} \\ \dot{\mathbf{a}}(t) &= -\mathbf{a}(t)^T \frac{\partial f(\mathbf{z}(t), \theta)}{\partial \mathbf{z}}, \end{aligned} \quad (10)$$

or in backward going time τ , the equation

$$\begin{aligned} \mathbf{a}(\tau = 0) &= \frac{\partial L}{\partial \mathbf{z}(\tau = 0)} \\ \dot{\mathbf{a}}(\tau) &= \mathbf{a}(\tau)^T \frac{\partial f(\mathbf{z}(\tau), \theta)}{\partial \mathbf{z}}. \end{aligned} \quad (11)$$

The total gradient of the loss function with respect to bias parameters is then obtained by

$$\frac{\partial L}{\partial \theta} = \int_0^{\tau_e} \mathbf{a}(\tau)^T \frac{\partial f(\mathbf{z}(\tau), \theta)}{\partial \theta} d\tau. \quad (12)$$

While solving (11), $z(\tau)$ can be either saved or reconstructed by running dynamics (3) backward, depending on the memory and computational trade-off we would like to maintain. The algorithm for running the adjoint method for the dynamics that include random noise is developed and analyzed in (Li et al., 2020).

3. Challenges and Solutions

3.1. Challenges

Ideally, one would simulate the biased dynamics (3), compute the loss (8), backpropagate by solving (11), and after a number of training epochs obtain the biasing potential that enhances transitions. However, differentiable simulations at their current state cannot be used out of the box. There exist several issues that need to be addressed.

1. Gradient control

Significant effort has been devoted in the past years to understand the gradients that arise while optimizing neural network controlled differentiable simulations (Suh et al., 2022; Huang et al., 2021; Metz et al., 2021). It is important to control the explosion or vanishing of gradients when training deep neural networks. A differentiable simulation can be arbitrarily deep, while the complex Hamiltonians can be challenging to backpropagate in a controllable manner. In fact, it is possible to construct a simple example of (3) that gives rise to exploding gradients by choosing a particular Hamiltonian (Galimberti et al., 2021).

2. Multiscale Problem

The dynamics on $U_0(x)$ can include very high and very low frequency motions. However, only the slow dynamics should be controlled by the trainable bias. High frequency modes, e.g., hydrogen vibrations in the case of molecules, do not contribute to the reaction mechanism. Fitting such fast fluctuations has to be avoided, which will reduce the noise in the gradients used for training.

3. Chaotic behaviour

One important property of some Hamiltonian systems is the emergence of chaos (Percival I, 1987). Small changes in initial conditions result in exponentially different trajectories. Great care must be taken to predict and control the behaviour of such systems.

4. One large parameter update per trajectory

Differentiable simulations in their original formulation produce one update per trajectory. Obtaining a sufficient number of gradient updates can be very expensive when long trajectories are required.

All these challenges are addressed by the present work.

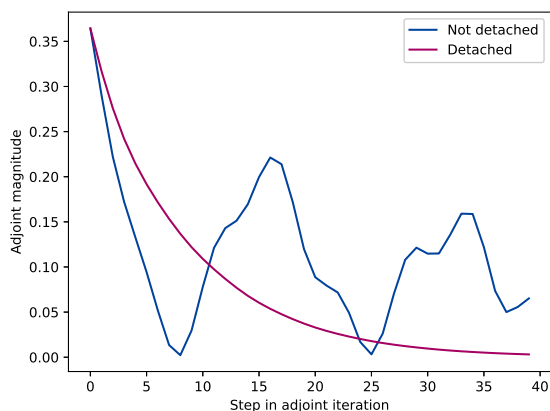


Figure 1: Comparison of the adjoint evolution for original and partially detached graphs for simulations on the 2D Müller-Brown potential with parameters given in Appendix F.

We show how to learn slow dynamics necessary for the investigation of chemical reactions while keeping gradients under control.

3.2. Partial backpropagation

To reduce the complexity and level of detail in the equations, the computational graph is pruned such that backpropagation occurs only in the momenta. This can be reasoned as follows:

- We consider the dynamics of our system to be Markovian, i.e., that there should be no explicit dependence on the history of x . As it is common, the bias potential B only depends on x and not p . Positions and momenta are coupled through the equations of motion.
- Since we want to optimize the movement towards the target, it is essential to optimize the dynamics, so the movement described by p .
- The use of the detach operator reduces the backpropagated ODE to first order in time, neglecting all higher order terms. Hence, the backpropagation is diffusive, and any oscillations are removed. The change in adjoint dynamics can be seen in the Figure 1.
- The removal of potentially diverging higher order terms makes the gradients well bounded and easy to calculate.

The `.detach()` operator introduced, e.g., in Refs. (Foerster et al., 2018; Schulman et al., 2015; Zhang et al., 2019), stops the flow of the gradient through x . This reduces the number

of equations for which the adjoint is calculated and through which is backpropagated. To derive the adjoint equation for this modified system, we use the equation:

$$\mathbf{x}(\tau) = \mathbf{x}(\tau - d\tau).detach() + \mathbf{p}(\tau)d\tau \quad (13)$$

The use of the detach operator simplifies the adjoint time derivative to

$$\begin{aligned} \dot{\mathbf{a}}(\tau) &= \mathbf{a}^T \frac{\partial}{\partial \mathbf{p}(\tau)} \left(-\frac{\partial U(\mathbf{x}(\tau))}{\partial \mathbf{x}} - \gamma \mathbf{p}(\tau) + \sqrt{2\gamma k_B T} \mathbf{R}(\tau) \right) \\ &= -\mathbf{a}^T(\tau) \left(\frac{\partial^2 U(\mathbf{x}(\tau))}{\partial^2 \mathbf{x}} \frac{\partial \mathbf{x}(\tau)}{\partial \mathbf{p}(\tau)} - \gamma \mathbf{I} \right) \\ &= -\mathbf{a}^T(\tau) \frac{\partial^2 U(\mathbf{x}(\tau))}{\partial^2 \mathbf{x}} d\tau - \gamma \mathbf{a}(\tau). \end{aligned} \quad (14)$$

Let us now formulate the property of the adjoints that will be useful when designing numerical methods and also gives us some assurance of the non-diverging gradient dynamics. Consider a trajectory \mathbf{x}_t generated by (3) with time t in a possibly infinite time interval $I \subset (-\infty, \infty)$. The loss (8) is defined for a point \mathbf{x}_{t_L} . To optimize $B(\mathbf{x}, \theta)$, we need to backpropagate the gradient of this loss through every point proceeding \mathbf{x}_{t_L} , using backwards flowing time τ . To summarize the notation and prepare to show some important properties, we present the following definitions.

Definition 3.1 (Differentiable Trajectory). A Differentiable Trajectory \mathcal{T} is defined by the following quadruple $(z(t), L(z(t_L)), f(z(t)), \tilde{f}(z(t)))$: Let $z(t) \in \Omega_{\mathbf{x}} \times \Omega_{\mathbf{p}}$ where $\Omega_{\mathbf{x}} \subset \mathbb{R}^N$ and $\Omega_{\mathbf{p}} \subset \mathbb{R}^N$ for $t \in (t_i, t_e)$, where $-\infty \leq t_i < t_e \leq \infty$ be the sequence of states generate by the dynamics $f(z(t))$ from a certain initial state $z(t_0), t_0 \in [t_i, t_e]$. We define a loss function $L(z(t_L))$ in time t_L . The gradient dynamics of the loss function is guided by the dynamics $\tilde{f}(z(t))$ that includes possible `.detach()` operators. The backward dynamics is represented in the reverse flowing time τ starting from $z(t_L) = z(\tau = 0)$ to $z(\tau_e) = z(t_i)$.

And we define a Diffusive Differentiable Trajectory by

Definition 3.2 (Diffusive Differentiable Trajectory). A Differentiable Trajectory \mathcal{T} constructed by dynamics (3) with a backward dynamics (14) and a loss function (8) is called a Diffusive Differentiable Trajectory, denoted by \mathcal{T}_d .

Property 1 (Finite gradient update). *Let γ be sufficiently high. Let*

$$U(\mathbf{x}) \in C^2(\Omega_{\mathbf{x}}) \text{ and } \frac{\partial f(z(\tau), \theta)}{\partial \theta} \in L^\infty(\Omega_{\mathbf{x}} \times \Omega_{\mathbf{p}}). \quad (15)$$

Then the gradient update for a loss function in a Diffusive Differentiable Trajectory is finite for every (possibly infinite) τ_e .

The essence of the proof and specification of the sufficient conditions for γ are addressed in the following theorem.

Theorem 3.3 (Converging adjoints). *\mathcal{T}_d be a Diffusive Differentiable Trajectory. Let $U(\mathbf{x}) \in C^2(\Omega_{\mathbf{x}})$ and denote the spectrum of its hessian $\frac{\partial^2 U(\mathbf{x}(t))}{\partial^2 \mathbf{x}}$ by $\lambda_i(\mathbf{x}(t))$. Define λ_{min} as*

$$\lambda_{min} = \inf_{\tau > 0} \min_i \lambda_i(\mathbf{x}(\tau)). \quad (16)$$

Then for every γ that fulfills: $(d\tau \lambda_{min} + \gamma) = \epsilon > 0$, it holds:

$$\forall \tau > 0 : \|\mathbf{a}(\tau)\|^2 \leq \|\mathbf{a}(0)\|^2 e^{-2\epsilon\tau} \quad (17)$$

We proof the theorem in the Appendix A. There is a useful corollary of the above

Corollary 3.4. *Under the assumptions of the theorem 3.3, $\|\mathbf{a}(\tau)\| \in L^r(0, \tau_e)$, $r \in [1, \infty]$.*

Proof. Case $r = \infty$ is trivial as the square root of the upper bound (17) is still finite $\forall \tau$. Let us now consider only $r \in [1, \infty)$.

$$\begin{aligned} \|\mathbf{a}(\tau)\|_{L^r(0, \tau_e)}^r &= \int_0^{\tau_e} \|\mathbf{a}(\tau)\|^r \leq \|\mathbf{a}(0)\|^r \int_0^{\tau_e} e^{-\epsilon r \tau} \\ &= -\frac{\|\mathbf{a}(0)\|^r}{\epsilon r} [e^{-\epsilon r \tau}]_0^{\tau_e} \end{aligned} \quad (18)$$

Which is finite for every value of τ_e including ∞ . \square

Proof of the finite gradient update 1. Since we know that $\mathbf{a}(\tau) \in L^1(0, \tau_e)$ from the previous corollary and that $\frac{\partial f(z(\tau), \theta)}{\partial \theta} \in L^\infty(\Omega_{\mathbf{x}} \times \Omega_{\mathbf{p}})$ from the assumption, it is now trivial to show

$$\begin{aligned} \frac{\partial L(z_{t_L})}{\partial \theta} &= \int_0^{\tau_e} \mathbf{a}(\tau) \frac{f(z(\tau), \theta)}{\partial \theta} d\tau \\ &\leq \sup_{z(\tau) \in T} \left\| \frac{\partial f(z(\tau), \theta)}{\partial \theta} \right\| \int_0^{\tau_e} \mathbf{a}(\tau) d\tau, \end{aligned} \quad (19)$$

which is finite. \square

This property allows us to backpropagate the dynamics without exploding gradients as long as γ is chosen large enough. The exponential scaling of the adjoints also indicates that once we identify the point where the loss function will be calculated, we only need to consider a handful of points before $\mathbf{a}(\tau)$ essentially vanishes. Any further adjoint propagation does not significantly contribute to the gradient update. This is intuitively desirable, as for the noisy equation (3) the loss function information becomes diluted as we backpropagate. Keeping only recent data points thus introduces a natural cutoff to the information we use for optimization.

The theorem also gives more insight into when such backpropagation may lead to exploding gradients. If the expression $(d\tau \lambda_{min} + \gamma) = \epsilon < 0$, then the upper bound may

not hold, and gradients can increase exponentially. Strongly negative λ_i of the hessian indicates a concave part in the potential landscape, which is generally problematic for control.

3.3. Mini batching the graph

One of the problems associated with differentiable simulation is the low number of updates. Usually, only one gradient step is taken per trajectory, making the gradients averaged across the entire path and necessitating rather large learning rates to train the network in just a few updates. The problem can be alleviated by a technique we call *graph mini batching*. The idea is to calculate trajectory depended gradients first (the adjoints α) in one pass and then split them to mini batches. The adjoints are then used as vectors in Jacobi-vector products (12) during backpropagation of the bias function evaluated in batches. The approach stabilizes learning and allows for much lower learning rates, better suited for training neural networks. An example of a use case is more thoroughly discussed in Appendix B.

3.4. Summary

The use of the Langevin thermostat with reasonable γ creates finite memory dynamics and therefore decaying adjoints. Employing also the `.detach()` operator ensures that the adjoints do vanish smoothly, without high frequency oscillations, thus making them bounded (solving Item 1) and ignoring fast motion, helping with Item 2. Such a finite memory system is likely to be less chaotic, addressing Item 3. Splitting the loss gradient into random mini-batches obviously solves the point 4.

4. Practical implementation

It is important to promote the transition across the barrier equally. If only one direction is sampled, then one may end up with a "landslide" potential strongly tilted towards one minimum and not a diffusive behaviour. Therefore, we choose the following approach.

1. Create a batch of $2l$ starting configurations, with l in each well respectively.
2. Run all trajectories simultaneously for a fixed number of time steps.
3. Collect the loss 8 after all simulations have ended. After N initial steps, which serve as equilibration, we also calculate the minimal distance from the start to encourage the eventual return to the starting well and, thereby, true diffusive behavior. Thus, we have two losses: A forward loss $L_f(\mathbf{x}_{L_f})$ and start loss $L_s(\mathbf{x}_{L_s})$.
4. Calculate adjoints and optimize the bias function

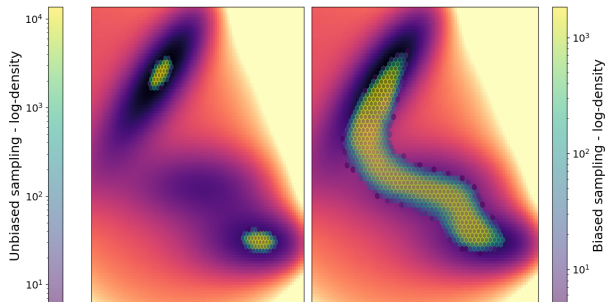


Figure 2: Log-density of simulated points before (*left*) and after the training (*right*) of bias function by differentiable simulations. The right plot shows how well all important regions are sampled after training. The background of the Figure is the $U_{MB}(x, y)$, the underlying Muller-Brown potential.

$B(\mathbf{x}, \theta)$ using the graph mini batching technique. Repeat from step 1 until convergence.

By running a large number of simulations concurrently, one can leverage the vectorization of the operations and reduce computational time.

5. Results

In this Section, we present the results of our differentiable simulation setup. First, we apply it to a commonly used, notorious two dimensional PES, the Muller-Brown potential (Müller & Brown, 1979), where any linear combination of the Cartesian coordinates does not yield a good CV. Then we lift this example to five dimensions by introducing three noisy DoFs demonstrating the efficiency and basic functionality of the approach.

Second, we investigate the golden standard for enhanced sampling in molecular systems, alanine dipeptide (amino acid alanine capped at both ends). The two collective variables describing the metastable states are well known in the community, the backbone dihedrals ϕ and ψ . We will assume no such knowledge and generate the enhanced sampling simulation from all backbone dihedral angles as candidates in an end-to-end process.

5.1. 2D Muller-Brown potential

The parameters of the commonly investigated 2D Muller-Brown PES (Müller & Brown, 1979; Sun et al., 2022) are given in the Appendix C. The simulation details are reported in Appendix C. For the bias potential, $B(\mathbf{x}, \mathbf{h})$, we employ a grid of Gaussian functions, controlling their individual

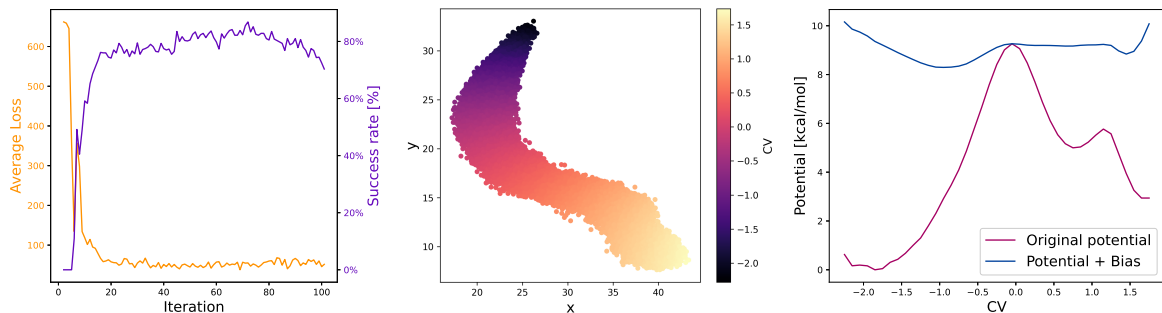


Figure 3: Postprocessing of the converged trajectory. *left*: Loss functions and the probability of barrier crossing during the training progresses. *middle*: Variational Autoencoder producing a collective variable by training on a fully diffusive trajectory. *right*: Potential energy along the VAE collective variable with and without bias.

height. The biasing function is

$$B(\mathbf{x}, \mathbf{h}) = \sum_{i=1}^{n_g} h_i \exp\left(-\frac{(\mathbf{x} - \mathbf{x}_i^0)^2}{2\sigma^2}\right) \quad (20)$$

with trainable \mathbf{h} . Means \mathbf{x}_i^0 are evenly distributed in the computational domain. In two dimensions, we can afford such a setup; with a reasonable number n_g of Gaussians along each dimension, we only need to calculate n_g^2 contributions to the total bias. As this approach scales exponentially with the dimensionality of the problem, it cannot be used with the 5D version of the potential (Appendix D). After training the bias via differentiable simulation with parameters reported in Appendix F, we obtain biased dynamics that generate a lot of successful transitions between reactants and products along the transition path. The log-density of the points along the transition path is also much more level Figure 2. The evolution of loss function and success rate during training are shown in Figure 3.

Following our philosophy of having CVs determined from well sampled transitions, we construct the collective variable by dimensionality reduction of converged diffusive trajectories. To obtain a single value collective variable describing the path, we use a Variational Autoencoder (Kingma & Welling, 2013). A very simple setup is employed with a two hidden layer encoder and a two hidden layer decoder, both with 50 hidden neurons and a Softplus activation function. The resulting CV is visualized in Figure 3. The CV distinguishes well and interpolates smoothly between products and reactants. Using the CV, the unbiased and biased PES are plotted as averages along the CV. It is easy to see in Figure 3 how effectively the PES has been flattened by the bias function.

5.2. 5D Generalization

The situation is more complicated when we include additional degrees of freedom that are harmonic and identical

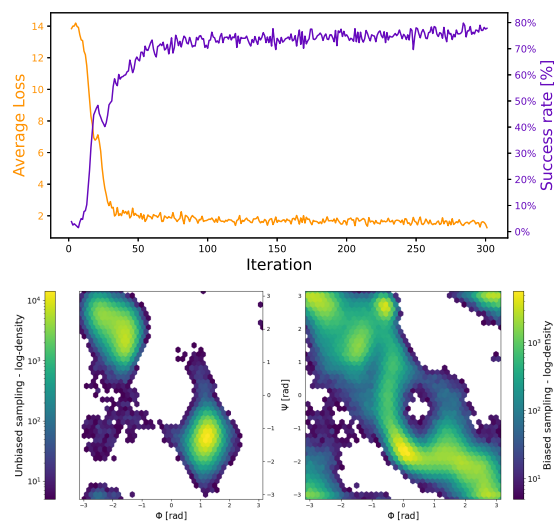


Figure 4: *top row*: Metrics for the alanine dipeptide run. Total loss function and transition success rate. *bottom row*: Log-density of simulated points before the training of bias by differentiable simulations (*left*) and after the training converged (*right*).

for both reactants and products. One may consider them to be, e.g., quickly oscillating hydrogen atoms that do not influence the reaction (see Appendix D for details regarding extended potential). In five dimensions, the grid of Gaussian basis functions is not feasible due to the exponential computational complexity. Instead, we employed a fully connected neural network as a function of all five variables, which made training significantly harder. For the results postprocessing we employ the same approach as in the two dimensional case. See Figure 7.

5.3. Alanine dipeptide

Alanine dipeptide is a simple model system exhibiting typical protein dihedral dynamics. Therefore, it has become an

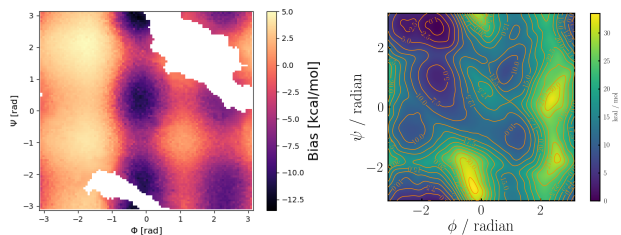


Figure 5: *left*: Average bias potential projected on the Ramachandran plane. White regions are without sufficient sampling to calculate bias potential. *right*: PMF of the ϕ - ψ -plane.

important benchmark to test and verify free energy calculation methods. The collective variables, the dihedral angles ϕ and ψ , are well known and the PES is rather complex with relatively low barriers. (Vymětal & Vondrášek, 2010; Mironov et al., 2019).

We use this system to test the ability of our method to bias the dynamics along the important DoFs. As candidate degrees of freedom, we choose four dihedral angles along the backbone of alanine dipeptide and one dihedral angle involving the methyl group that we expect to be correlated with ψ . In each dihedral angle, we define a Gaussian basis set, which accounts for periodicity. These expanded dihedrals are then input to a fully connected network that calculates the bias function. The detailed settings are listed in Appendix F.

As ϕ and ψ are known, the results are reported as Ramachandran plots. No additional dimensionality reduction via VAEs is performed.

By comparing the averaged bias potential with a potential of mean force (PMF) obtained with Metadynamics (see Appendix E) we can see that their shapes are similar. This demonstrates that our differentiable simulations can unravel the transition paths and reaction barriers in the same way as a collective variable based method would, except without requiring prior knowledge of ideal CVs.

The numerical tool used for the differentiable simulation of alanine dipeptide contained components modified from TorchMD library (Doerr et al., 2021). We, with some modifications, used mainly the Amber forcefield adapter written in PyTorch and some of the utilities for simulation setup. The forcefield used was Amber ff19SB (Tian et al., 2020). We simulated in vacuum.

The progress of the training and log-density of points are reported in Figure 4. The comparison of the obtained potential of the mean force is in the Figure 5.

6. Discussion

The proposed method can solve the problem of finding reaction paths and estimating barriers without prior knowledge of important degrees of freedom. In this section we discuss its main contributions to the topic of differentiable simulations, summarize theoretical results and outline possible limitations and further steps.

Path integral optimization: We formulate the loss function optimization as a minimization of a path dependent integral. The usefulness of differentiable simulations for such problems can be best understood on simple examples that contain path dependence explicitly. One such example, the famous Brachistochrone curve, the shortest path in a gravitational field, is included in the Appendix G. In our case, this means we can define the total loss for the simulated trajectory and translate how it can be minimized by modifying the bias in the preceding points.

Transition state identification: According to the Transition State Theory developed by Eyring and Polanyi (Laidler & King, 1983) the reaction path passes a saddle point on the potential energy surface (PES) called transition state. A successful method used to study reactions is expected to find the transition state at least approximately. We do not explicitly include any terms in the loss function to find the saddle point, although this would be a possibility. For the studied systems, it was sufficient to progressively decay the learning rate with an increasing success rate of the transition and therefore accumulate only just enough bias to cross freely. The transition state is then found naturally as a region with the lowest barrier for reactions.

Simulations with vanishing information: A vital concept we develop is the principle of finite time horizon influencing the loss function. We employ the detached Langevin dynamics and show that the friction term in the momentum equation gradually replaces the initial information with noise. This translates to adjoints exponentially vanishing and being effectively zero after a certain number of steps.

In this paper, we focused on method development and analyzed properties of differentiable simulations applied to the study of chemical systems. We have demonstrated that differentiable simulations with our innovations can handle not only model systems but also complex molecular motions. In the future, we intend to extend the tool to more challenging reactions with complicated transition paths, such as protein motion and chemical reactions with multiple intermediate steps or competing reaction paths.

Acknowledgements

M.S. was supported by project No. START/SCI/053 of Charles University Research program. J.C.B.D. is thank-

ful for the support of the Leopoldina Fellowship Program, German National Academy of Sciences Leopoldina, grant number LPDS 2021-08. R.G.-B. acknowledges support from the Jeffrey Cheah Career Development Chair.

References

- Abrams, C. and Bussi, G. Enhanced Sampling in Molecular Dynamics Using Metadynamics, Replica-Exchange, and Temperature-Acceleration. *Entropy* 2014, Vol. 16, Pages 163-199, 16(1):163–199, 12 2013. ISSN 1099-4300. doi: 10.3390/E16010163. URL <https://www.mdpi.com/1099-4300/16/1/163/html><https://www.mdpi.com/1099-4300/16/1/163>.
- Barducci, A., Bussi, G., and Parrinello, M. Well-Tempered Metadynamics: A Smoothly Converging and Tunable Free-Energy Method. *Physical Review Letters*, 100 (2):020603, 1 2008. ISSN 0031-9007. doi: 10.1103/PhysRevLett.100.020603.
- Bellman, R. Dynamic programming. *Mathematics in Science and Engineering*, 40(P1):101–137, 1967. ISSN 00765392. doi: 10.1016/S0076-5392(08)61063-2.
- Bonati, L., Rizzi, V., and Parrinello, M. Data-Driven Collective Variables for Enhanced Sampling. *The journal of physical chemistry letters*, 11(8):2998–3004, 4 2020. ISSN 1948-7185. doi: 10.1021/ACS.JPCLETT.0C00535. URL <https://pubmed.ncbi.nlm.nih.gov/32239945/>.
- Boyer, C. and Merzbach Uta. *A History of Mathematics, Second Edition*. Wiley, 2 edition, 3 1991.
- Callen, H. B. and Scott, H. L. *Thermodynamics and an Introduction to Thermostatistics, 2nd ed*, volume 66. 1998. doi: 10.1119/1.19071.
- Chen, R. T., Rubanova, Y., Bettencourt, J., and Duvenaud, D. Neural ordinary differential equations. In *Advances in Neural Information Processing Systems*, volume 2018-December, 2018a.
- Chen, W., Tan, A. R., and Ferguson, A. L. Collective variable discovery and enhanced sampling using autoencoders: Innovations in network architecture and error function design. *The Journal of Chemical Physics*, 149 (7):072312, 8 2018b. ISSN 0021-9606. doi: 10.1063/1.5023804.
- Chipot, C. Frontiers in free-energy calculations of biological systems. *Wiley Interdisciplinary Reviews: Computational Molecular Science*, 4(1):71–89, 1 2014. ISSN 1759-0884. doi: 10.1002/WCMS.1157. URL <https://onlinelibrary.wiley.com/doi/full/10.1002/wcms.1157><https://onlinelibrary.wiley.com/doi/abs/10.1002/wcms.1157><https://wires.onlinelibrary.wiley.com/doi/10.1002/wcms.1157>.
- Chipot, C. and Pohorille, A. *Free Energy Calculations*, volume 86 of *Springer Series in CHEMICAL PHYSICS*. Springer Berlin Heidelberg, Berlin, Heidelberg, 2007. ISBN 978-3-540-38447-2. doi: 10.1007/978-3-540-38448-9. URL <http://link.springer.com/10.1007/978-3-540-38448-9>.
- Darve, E. and Pohorille, A. Calculating free energies using average force. 2001. doi: 10.1063/1.1410978. URL <http://jcp.aip.org/jcp/copyright.jsp>.
- de Avila Belbute-Peres, F., Smith, K., Allen, K., Tenenbaum, J., and Kolter, J. Z. End-to-End Differentiable Physics for Learning and Control. In Bengio, S., Wallach, H., Larochelle, H., Grauman, K., Cesa-Bianchi, N., and Garnett, R. (eds.), *Advances in Neural Information Processing Systems*, volume 31. Curran Associates, Inc., 2018. URL <https://proceedings.neurips.cc/paper/2018/file/842424a1d0595b76ec4fa03c46e8d755-Paper.pdf>.
- Degrave, J., Hermans, M., Dambre, J., and wyffels, F. A Differentiable Physics Engine for Deep Learning in Robotics. 11 2016.
- Doerr, S., Majewski, M., Pérez, A., Krämer, A., Clementi, C., Noe, F., Giorgino, T., and De Fabritiis, G. TorchMD: A Deep Learning Framework for Molecular Simulations. *Journal of Chemical Theory and Computation*, 17(4): 2355–2363, 4 2021. ISSN 1549-9618. doi: 10.1021/acs.jctc.0c01343.
- Foerster, J., Farquhar, G., Al-Shedivat, M., Rocktäschel, T., Xing, E. P., and Whiteson, S. DiCE: The Infinitely Differentiable Monte-Carlo Estimator. 2 2018.
- Galimberti, C. L., Furieri, L., Xu, L., and Ferrari-Trecate, G. Hamiltonian Deep Neural Networks Guaranteeing Non-vanishing Gradients by Design. 5 2021.
- Greener, J. G. and Jones, D. T. Differentiable molecular simulation can learn all the parameters in a coarse-grained force field for proteins. *PLOS ONE*, 16(9):e0256990, 9 2021. ISSN 1932-6203. doi: 10.1371/journal.pone.0256990.
- Hu, Y., Li, T.-M., Anderson, L., Ragan-Kelley, J., and Durand, F. Taichi. *ACM Transactions on Graphics*, 38(6): 1–16, 12 2019. ISSN 0730-0301. doi: 10.1145/3355089.3356506.

- Hu, Y., Anderson, L., Li, T.-M., Sun, Q., Carr, N., Ragan-Kelley, J., and Durand, F. DiffTaichi: Differentiable Programming for Physical Simulation. In *International Conference on Learning Representations*, 2020. URL <https://openreview.net/forum?id=B1eB5xSFvr>.
- Huang, Z., Hu, Y., Du, T., Zhou, S., Su, H., Tenenbaum, J. B., and Gan, C. PlasticineLab: A Soft-Body Manipulation Benchmark with Differentiable Physics. In *International Conference on Learning Representations*, 2021. URL <https://openreview.net/forum?id=xCcdBRQEDW>.
- Ingraham, J., Riesselman, A., Sander, C., and Marks, D. Learning Protein Structure with a Differentiable Simulator. In *International Conference on Learning Representations*, 2019. URL <https://openreview.net/forum?id=Byg3y3C9Km>.
- Kingma, D. P. and Welling, M. Auto-Encoding Variational Bayes. 12 2013.
- Köppen, M. The curse of dimensionality. 2000.
- Laidler, K. J. and King, M. C. Development of transition-state theory. *The Journal of Physical Chemistry*, 87(15):2657–2664, 7 1983. ISSN 0022-3654. doi: 10.1021/j100238a002.
- Laio, A. and Parrinello, M. Escaping free-energy minima. *Proceedings of the National Academy of Sciences of the United States of America*, 99(20):12562–12566, 10 2002. ISSN 00278424. doi: 10.1073/PNAS.202427399/ASSET/2381B9FD-FD4C-4ED9-9DCB-75FD02E8EA7E/ASSETS/GRAPHIC/PQ2024273003.JPEG. URL <https://www.pnas.org/doi/abs/10.1073/pnas.202427399>.
- Lev Semenovich Pontryagin, MishGamkrelidze RV, Boltyanskii VG, and Gamkrelidze RV. *The Mathematical Theory of Optimal Processes*. 1962.
- Li, X., Wong, T.-K. L., Chen, R. T. Q., and Duvenaud, D. K. Scalable Gradients and Variational Inference for Stochastic Differential Equations. In *Proceedings of The 2nd Symposium on Advances in Approximate Bayesian Inference*, volume 118 of *Proceedings of Machine Learning Research*, pp. 1–28. PMLR, 9 2020. URL <https://proceedings.mlr.press/v118/li20a.html>.
- Mendels, D., Piccini, G., and Parrinello, M. Collective Variables from Local Fluctuations. *Journal of Physical Chemistry Letters*, 9(11):2776–2781, 6 2018. ISSN 19487185. doi: 10.1021/ACS.JPCLETT.8B00733/ASSET/IMAGES/LARGE/JZ-2018-00733T{_}0005.JPEG. URL <https://pubs.acs.org/doi/full/10.1021/acs.jpcllett.8b00733>.
- Mertens, S. and Mingramm, S. Brachistochrones with loose ends. *European Journal of Physics*, 29(6):1191–1199, 11 2008. ISSN 0143-0807. doi: 10.1088/0143-0807/29/6/008.
- Metz, L., Freeman, C. D., Schoenholz, S. S., and Kachman, T. Gradients are Not All You Need. 11 2021.
- Mironov, V., Alexeev, Y., Mulligan, V. K., and Fedorov, D. G. A systematic study of minima in alanine dipeptide. *Journal of Computational Chemistry*, 40(2):297–309, 1 2019. ISSN 0192-8651. doi: 10.1002/jcc.25589.
- Müller, K. and Brown, L. D. Location of saddle points and minimum energy paths by a constrained simplex optimization procedure. *Theoretica chimica acta*, 53(1):75–93, 1979. ISSN 1432-2234. doi: 10.1007/BF00547608. URL <https://doi.org/10.1007/BF00547608>.
- Percival I. Chaos in hamiltonian systems. *Proceedings of the Royal Society of London. A. Mathematical and Physical Sciences*, 413(1844):131–143, 9 1987. ISSN 0080-4630. doi: 10.1098/rspa.1987.0105.
- Schulman, J., Heess, N., Weber, T., and Abbeel, P. Gradient Estimation Using Stochastic Computation Graphs. 6 2015.
- Schwantes, C. R. and Pande, V. S. Modeling Molecular Kinetics with tICA and the Kernel Trick. *Journal of Chemical Theory and Computation*, 11(2):600–608, 2 2015. ISSN 1549-9618. doi: 10.1021/ct5007357.
- Šípka, M., Erlebach, A., and Grajciar, L. Understanding chemical reactions via variational autoencoder and atomic representations. 3 2022.
- Spiwok, V., Sucer, Z., and Hosek, P. Enhanced sampling techniques in biomolecular simulations. *Biotechnology advances*, 33(6 Pt 2):1130–1140, 2015. ISSN 1873-1899. doi: 10.1016/J.BIOTECHADV.2014.11.011. URL <https://pubmed.ncbi.nlm.nih.gov/25482668/>.
- Suh, H. J. T., Simchowit, M., Zhang, K., and Tedrake, R. Do Differentiable Simulators Give Better Policy Gradients? 2 2022.
- Sultan, M. M. and Pande, V. S. Automated design of collective variables using supervised machine learning. *The Journal of Chemical Physics*, 149(9):94106, 2018. doi: 10.1063/1.5029972. URL <https://doi.org/10.1063/1.5029972>.

- Sun, L., Vandermause, J., Batzner, S., Xie, Y., Clark, D., Chen, W., and Kozinsky, B. Multitask Machine Learning of Collective Variables for Enhanced Sampling of Rare Events. *Journal of Chemical Theory and Computation*, 18(4):2341–2353, 2022. doi: 10.1021/acs.jctc.1c00143. URL <https://doi.org/10.1021/acs.jctc.1c00143>.
- Tian, C., Kasavajhala, K., Belfon, K. A. A., Raguetto, L., Huang, H., Miguies, A. N., Bickel, J., Wang, Y., Pincay, J., Wu, Q., and Simmerling, C. ff19SB: Amino-Acid-Specific Protein Backbone Parameters Trained against Quantum Mechanics Energy Surfaces in Solution. *Journal of Chemical Theory and Computation*, 16(1):528–552, 1 2020. ISSN 1549-9618. doi: 10.1021/acs.jctc.9b00591.
- Torrie, G. M., Valleau, J. P., Torrie, G. M., and Valleau, J. P. Nonphysical Sampling Distributions in Monte Carlo Free-Energy Estimation: Umbrella Sampling. *JCoPh*, 23(2):187–199, 1977. ISSN 0021-9991. doi: 10.1016/0021-9991(77)90121-8. URL <https://ui.adsabs.harvard.edu/abs/1977JCoPh..23..187T/abstract>.
- Valsson, O., Tiwary, P., and Parrinello, M. Enhancing Important Fluctuations: Rare Events and Metadynamics from a Conceptual Viewpoint. <http://dx.doi.org/10.1146/annurev-physchem-040215-112229>, 67:159–184, 5 2016. ISSN 0066426X. doi: 10.1146/ANNUREV-PHYSCHEM-040215-112229. URL <https://www.annualreviews.org/doi/abs/10.1146/annurev-physchem-040215-112229>.
- Vymětal, J. and Vondrášek, J. Metadynamics As a Tool for Mapping the Conformational and Free-Energy Space of Peptides — The Alanine Dipeptide Case Study. *The Journal of Physical Chemistry B*, 114(16):5632–5642, 4 2010. ISSN 1520-6106. doi: 10.1021/jp100950w.
- Wang, D. and Tiwary, P. State predictive information bottleneck. *The Journal of Chemical Physics*, 154(13):134111, 4 2021. ISSN 0021-9606. doi: 10.1063/5.0038198. URL <https://aip.scitation.org/doi/abs/10.1063/5.0038198>.
- Wang, W., Axelrod, S., and Gómez-Bombarelli, R. Differentiable Molecular Simulations for Control and Learning. 2 2020.
- Wang, Y., Ribeiro, J. M. L., and Tiwary, P. Past–future information bottleneck for sampling molecular reaction coordinate simultaneously with thermodynamics and kinetics. *Nature Communications* 2019 10:1, 10(1):1–8, 8 2019. ISSN 2041-1723. doi: 10.1038/s41467-019-11405-4. URL <https://www.nature.com/articles/s41467-019-11405-4>.
- Wehmeyer, C. and Noé, F. Time-lagged autoencoders: Deep learning of slow collective variables for molecular kinetics. *The Journal of Chemical Physics*, 148(24):241703, 2018. doi: 10.1063/1.5011399. URL <https://doi.org/10.1063/1.5011399>.
- Zhang, S.-X., Wan, Z.-Q., and Yao, H. Automatic Differentiable Monte Carlo: Theory and Application. 11 2019.

A. Proof of adjoint convergence theorem

To prove Theorem 3.3 we need to state one more lemma.

Lemma A.1. *Let $\mathbf{x} \in \mathbb{R}^N$, $U(\mathbf{x})$ scalar, real, $C^2(\mathbb{R}^N)$ function. Consider a hessian computed at \mathbf{x}_0 : $\frac{\partial^2 U(\mathbf{x}_0)}{\partial \mathbf{x}^2}$ with minimum and maximum eigenvalues λ_{min} and λ_{max} respectively. Then for any vector $\mathbf{v} \in \mathbb{R}^N$*

$$\lambda_{min} \|\mathbf{v}\|^2 \leq \mathbf{v}^T \cdot \frac{\partial^2 U(\mathbf{x}_0)}{\partial \mathbf{x}^2} \mathbf{v} \leq \lambda_{max} \|\mathbf{v}\|^2. \quad (21)$$

Proof. We note that a hessian of a real continuous function is a symmetric matrix. Such a matrix is orthogonally diagonalizable and has real eigenvalues. The rest of the proof is a part of most standard linear algebra textbooks. \square

We can now prove the Theorem 3.3.

Proof. We start by multiplying (14) by $2\mathbf{a}$. This yields

$$2\mathbf{a}(\tau) \cdot \dot{\mathbf{a}}(\tau) = 2d\tau \mathbf{a}^T(\tau) \cdot \frac{\partial^2 U(\mathbf{x}(\tau))}{\partial^2 \mathbf{x}} \mathbf{a}(\tau) - 2\gamma \|\mathbf{a}(\tau)\|^2 \quad (22)$$

and can be recast using $2\mathbf{a}^T(\tau) \cdot \dot{\mathbf{a}}(\tau) = \frac{d}{dt} \|\mathbf{a}(\tau)\|^2$ (the norm is a standard vector 2-norm) to

$$\frac{d}{dt} \|\mathbf{a}(\tau)\|^2 = -2d\tau \mathbf{a}^T(\tau) \cdot \frac{\partial^2 U(\mathbf{x}(\tau))}{\partial^2 \mathbf{x}} \mathbf{a}(\tau) - 2\gamma \|\mathbf{a}(\tau)\|^2 \quad (23)$$

Using Lemma A.1 and, subsequently, the assumption of the theorem, we can estimate the upper bound of the time derivative as

$$\frac{d}{dt} \|\mathbf{a}(\tau)\|^2 \leq -2(d\tau \lambda_{min} + \gamma) \|\mathbf{a}(\tau)\|^2 = -2\epsilon \|\mathbf{a}(\tau)\|^2 \quad (24)$$

Using Gromwall lemma we can now estimate $\mathbf{a}(\tau)$ easily as

$$\|\mathbf{a}(\tau)\|^2 \leq \|\mathbf{a}(0)\|^2 \exp\left(-2 \int_0^\tau \epsilon dt\right) = \|\mathbf{a}(0)\|^2 e^{-2\epsilon\tau} \quad (25)$$

and since $\epsilon > 0$, the $\|\mathbf{a}(\tau)\|^2$ is bounded for all τ . \square

B. Graph minibatching and adjoints

To better explain the graph minibatching technique, let us consider a simple differential equation with trainable parameters θ

$$\dot{z} = f(z, \theta) \quad (26)$$

Let us discretize the equation using a simple Forward Euler method such that it becomes

$$z_{n+1} = z_n + dt f(z_n, \theta). \quad (27)$$

For simplicity consider a three step differentiable simulation (z_0, z_1, z_2) such that

$$\begin{aligned} z_2 &= z_1 + dt f(z_1, \theta) \\ z_1 &= z_0 + dt f(z_0, \theta) \end{aligned}$$

where a loss function is defined for the last point $L(z_2)$. Our goal is to find the gradient of $\frac{\partial L(z_2)}{\partial \theta}$. Let us derive

$$\begin{aligned} \frac{\partial L(z_2)}{\partial \theta} &= \frac{\partial L(z_2)}{\partial z_2} \frac{\partial z_2}{\partial \theta} \\ \frac{\partial z_2}{\partial \theta} &= \frac{\partial z_1}{\partial \theta} + dt \frac{\partial f(z_1, \theta)}{\partial \theta} = \frac{\partial z_1}{\partial \theta} + dt \left(\frac{\partial f(z_1, \theta)}{\partial z_1} \frac{\partial z_1}{\partial \theta} + \frac{\partial f(z_1, \theta)}{\partial \theta} \right) \\ \frac{\partial z_1}{\partial \theta} &= \frac{\partial z_0}{\partial \theta} + dt \frac{\partial f(z_0, \theta)}{\partial \theta} = dt \frac{\partial f(z_0, \theta)}{\partial \theta}. \end{aligned}$$

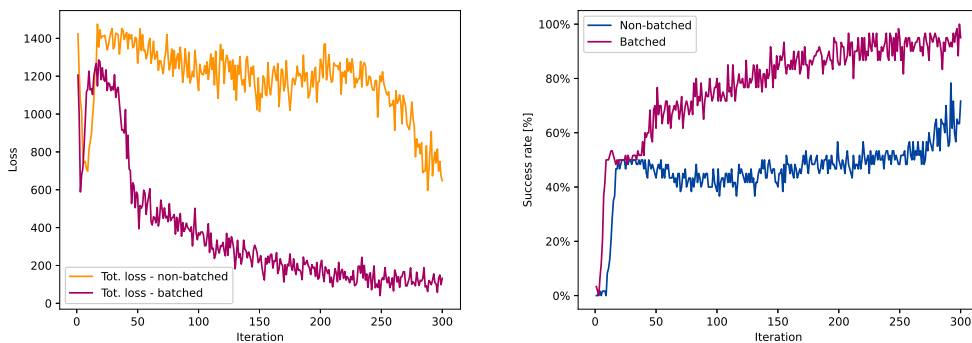


Figure 6: Comparison of the batched and one-time update of the weights in the 2D example from 5.1. The learning rate for the unbatched example was set approximately a number of batches times larger than for the batched run. The convergence is clearly more stable and even faster in the batched case. This was also observed for any other setting we tried during the development.

Put together,

$$\frac{\partial L(z_2)}{\partial \theta} = \frac{\partial L(z_2)}{\partial z_2} \left[dt \left(1 + dt \frac{\partial f(z_1, \theta)}{\partial z_1} \right) \frac{\partial f(z_0, \theta)}{\partial \theta} + dt \frac{\partial f(z_1, \theta)}{\partial \theta} \right]. \quad (28)$$

Meaning, when we optimize the biased function $f(z_n, \theta)$ We can split the derivative into two parts

$$\begin{aligned} & \left[\frac{\partial L(z_2)}{\partial z_2} dt \left(1 + dt \frac{\partial f(z_1, \theta)}{\partial z_1} \right) \right] \frac{\partial f(z_0, \theta)}{\partial \theta} \\ & \left[\frac{\partial L(z_2)}{\partial z_2} dt \right] \frac{\partial f(z_1, \theta)}{\partial \theta} \end{aligned} \quad (29)$$

More steps can be obtained by continuing the iterations. One can easily see that the vectors we put into square brackets are actually the adjoints $a(z_n)$ from (11). By saving these vectors, we can then take z_n , feed forward through $f(z_n, \theta)$ and backpropagate using the vector jacobian product. This can be done in one gradient update, accumulating a gradient with respect to θ and updating it after going through all adjoints, or we can update weights in batches as it is common in neural network training. The latter is shown to be the more stable and faster converging of the methods (see Figure 6).

C. 2D Muller-Brown potential

The equation of the PES:

$$U_{\text{MB}}(x, y) = B \sum_{i=1}^4 A_i \exp [\alpha_i (x - x_0)^2 + \beta_i (x - x_0)(y - y_0) + \gamma_i (y - y_0)^2] \quad (30)$$

The parameters used in this work are:

i	A_i	α_i	β_i	γ_i	x_0	y_0
1	-1.73	0	-0.39	-3.91	48	8
2	-0.87	0	-0.39	-3.91	32	16
3	-1.47	4.3	-2.54	-2.54	24	31
4	0.13	0.23	0.273	0.273	16	24

The barrier parameter $B = 10$ kcal/mol

D. 5D Generalization

We consider a generalization of the Muller-Brown potential. By adding three harmonic DoFs we complicate the problem and make it necessary to use a general form of a biasing potential, dependent on all degrees of freedom, as we do not know

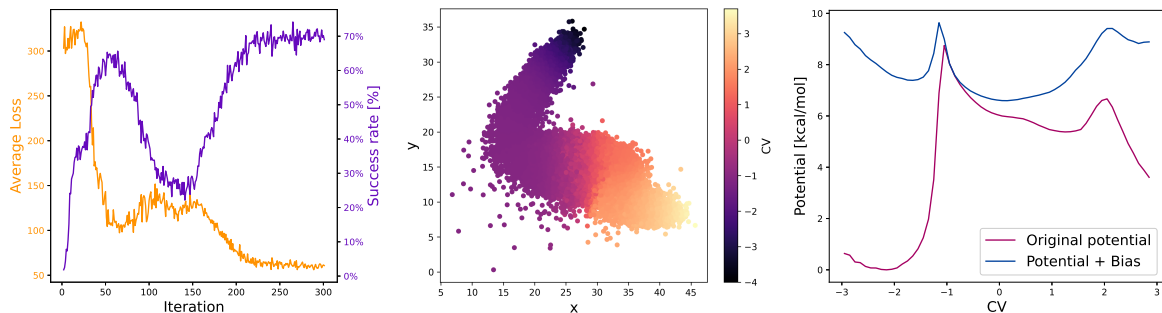


Figure 7: Results for the 5D extension of the Muller-Brown potential. *left*: Evolution of loss value and probability of barrier crossing during the training progresses. *middle*: CV determined with a Variational Autoencoder trained on a fully diffusive trajectory. The collective variables are not sharp around the transition region due to the high variance of the other noisy DoFs. This could be improved by more data, and more refined dimensionality reduction techniques that include temporal data such as e.g TiCA (Schwantes & Pande, 2015) or time-lagged autoencoders (Wehmeyer & Noé, 2018). *right*: Average potential energy along the VAE collective variable with and without bias. The barriers were lowered to the level where they could be crossed with high probability.

which of them defines the reaction. The resulting potential has the form:

$$U_{5D}(x_1, x_2, x_3, x_4, x_5) = U_{MB}(x_1, x_3) + \kappa(x_2^2 + x_4^2 + x_5^2) \quad (31)$$

The parameters for $U_{MB}(x_1, x_3)$ are identical to the 2D-case, the new parameter $\kappa = 0.1$. The results for the 5D case are visualized in the figure Figure 3.

E. Alanine dipeptide simulation settings

The PMF of alanine dipeptide was obtained by means of well-tempered metadynamics (Barducci et al., 2008). The deposited Gaussians had an initial height of 1 kcal/mol, a width of 10° along both dihedrals, and were deposited every 50 fs. The WTMetaD temperature was 4000 K. The simulation time step was 1 fs and the temperature was kept at 300 K with the Langevin thermostat with a friction constant of 1 ps^{-1} . The total simulation time was 50 ns.

F. Differentiable simulation parameters

The equations we simulate are (3), discretized by the Leapfrog algorithm. The method is symplectic and conserves energy. The constants and parameters of the method were chosen as follows:

case	m [g/mol]	γ [ps^{-1}]	T [K]	dt [fs]	timesteps	epochs
2D	0.1	0.1	10	1	6000	101
5D	0.01	1.0	300	1	20 000	65
Ala2	-	0.1	300	1	10 000	301

The column "timesteps" lists for how many steps we propagate a single simulation in each epoch. The update of parameters then represents an epoch. For the backward dynamics, we use 190 adjoints directly before the point where the loss function is calculated.

Batches of Parallel MDs These batches refer to the number of replicas that are simulated simultaneously. Using GPUs, we can parallelize the computation of forces and time step integration and thus are able to run 600 systems at once with a similar speed of running just one. Accumulating the simulated data from so many systems allows us to increase the number of adjoints obtained and enables us to use a lower learning rate, making the training more stable.

The setup of the bias function differed for every test case:

2D Muller-Brown: In this case, we use the setup described in (20) with 50 times 50 basis functions.

5d Muller-brown: We use a fully connected network with all five degrees of freedom used as five continuous input neurons.

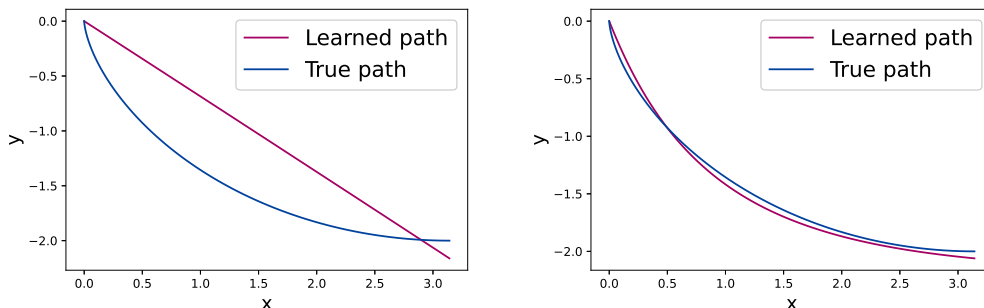


Figure 8: *left* Initial state. The path is initialized as an almost straight path. *right* After 200 iterations of differentiable simulations training, the path approximates the true path. The difference between the true curve and the one obtained by training is likely in the numerical scheme used to evaluate the integral.

The network has four hidden layers, each 150 neurons with SiLU as activation functions. The final layer has a single output neuron - the bias - and no activation.

Alanine dipeptide: In the case of real molecules, the bias function gets more complicated. We define the Gaussian basis set in every single degree of freedom represented by a basis vector \mathbf{e}_j and form a vector

$$\mathbf{v}(\mathbf{x}) = \sum_{j=1}^{n_{dof}} \sum_{i=1}^{n_g} \exp\left(-\frac{(\mathbf{x} - \mathbf{x}_{ij}^0)^2}{2\sigma^2}\right) \mathbf{e}_j. \quad (32)$$

n_{dof} represents the total number of candidate CVs or degrees of freedom considered. In our case, this was 5. n_g is the total number of basis functions defined separately for every candidate CV. In our case, this was 50 and since we described dihedral angles, centers \mathbf{x}_{ij}^0 were distributed uniformly from 0 to 2π , respecting the periodicity of dihedrals. The flattened vector $\mathbf{v}(\mathbf{x})$ with size $n_{dof} \cdot n_g$ is then used as an input to a fully connected neural network with three hidden layers, each 150 neurons with SiLU as an activation function. The final layer has one output neuron without an activation function.

Graph-Minibatching batch size This batch size refers to the mini-batching of the computational graph illustrated in Appendix B. Here we split the accumulated adjoints into smaller batches and train the network sequentially. The mini-batch of 120 was used for all systems. We use the learning rate as a learning factor divided by the number of replicas to make it independent of the number of systems simulated simultaneously. The learning factor is chosen as 10 for the 2D case, $\frac{1}{5}$ for the 5D case and 3 for the Alanine dipeptide. This, with 300 replicas running from reactant to the product and 300 the other way, gives us learning rates on the orders 10^{-2} to 10^{-3} . We use Adam optimizer for all our cases.

G. Brachistochrone curve

Here we exemplify how one can employ differentiable simulations and their capabilities to optimize path dependent integrals and solve the Brachistochrone problem. The problem is formulated as follows: Given a mass freely sliding on a curve $y = y(x)$ in the gravitational field g , find the curve from point **A** to lower point **B** for which the sliding time is the shortest. We assume no friction or air resistance and assume that **B** does not lie directly below **A**. For simplicity, we choose **A** to be the origin of the coordinate system. The solution, the cyclone curve, of this famous problem was obtained by Leibniz, L'Hospital, Newton, and Bernoulli brothers (Boyer & Merzbach Uta, 1991). A modified version, where we allow for an arbitrary difference in height between the two points and only prescribe their horizontal distance Δx was solved by Lagrange and much later summarized and written in the modern language of variational formalism by (Mertens & Mingramm, 2008). In this case, a solution is also a cyclone with some parameters fixed. We prescribe the horizontal Δx to be π and search for a solution using differentiable simulations. A simple fully connected neural network $f(x)$ serves as a derivative of the curve $f(x) = \frac{dy(x)}{dx}$, so that $y(x)$ is then obtained by the path integration of the neural network. After integration, we numerically evaluate the time from the simulated path

$$t = \int_0^\pi \frac{dx}{v} = \int_0^\pi \sqrt{\frac{1 + \left(\frac{dy(x)}{dx}\right)^2}{-2gy(x)}} dx \quad (33)$$

and minimize it. The formula can be easily derived from the conservation of kinetic energy and from a Pythagorean expression $ds^2 = dx^2 + dy^2$. For the path construction and backpropagation we employ the *torchdiffeq* python package shipped with the paper (Chen et al., 2018a).

In this example, we present a problem that could not be solved with just a point-wise neural network optimization but requires consideration of a full path.